Femtosecond laser induced surface swelling in poly-methyl methacrylate

Farhana Baset, Konstantin Popov, Ana Villafranca, Jean-Michel Guay, Zeinab Al-Rekabi, Andrew E. Pelling, Lora Ramunno and Ravi Bhardwaj*

Department of Physics, University of Ottawa, 150 Louis Pasteur, Ottawa, ON, K1N 6N5, Canada

**ravi.bhardwaj@uottawa.ca*

Abstract: We show that surface swelling is the first step in the interaction of a single femtosecond laser pulse with PMMA. This is followed by perforation of the swollen structure and material ejection. The size of the swelling and the perforated hole increases with pulse energy. After certain energy the swelling disappears and the interaction is dominated by the ablated hole. This behaviour is independent of laser polarization. The threshold energy at which the hole size coincides with size of swelling is 1.5 times that of the threshold for surface swelling. 2D molecular dynamics simulations show surface swelling at low pulse energies along with void formation below the surface within the interaction region. Simulations show that at higher energies, the voids coalesce and grow, and the interaction is dominated by material ejection.

OCIS codes: (140.3390) Laser material processing; (220.4241) Nanostructure fabrication; (320.2250) Femtosecond phenomena.

References and links

1. C. D. Marco, S. M. Eaton, R. Suriano, S. Turri, M. Levi, R. Ramponi, G. Cerullo, and R. Osellame, "Surface properties of femtosecond laser ablated PMMA," Appl. Mater. Interfaces **8**, 2377–2384 (2010)
2. E. Yap, D. G. McCulloch, D. R. McKenzie, M. V. Swain, L. S. Wielunski, and R. A. Clissold, "Modification of the mechanicaland optical properties of polycarbonate by 50-keV Ar^+ and H^+ ion implantation," J. Appl. Phys. **83**, 3404–3412 (1998)
3. S. Nolte, B. N. Chichkov, H. Welling, Y. Shani, K. Liebermann, and H. Terkel, "Nanostructuring with spatially localized femtosecond laser pulses," Opt. Lett. **24**, 914–916 (1999)
4. J. Kruger and W. Kautek, "The femtosecond pulse laser: a new tool for micromaching," Laser Phys. **9**,30–40 (1999).
5. K. M. Davis, K. Miura, N. Suguimoto, and K. Hirao, "Writing waveguides in glass with a femtosecond laser," Opt. Lett. **21**, 1729 (1996)
6. E.N. Glezer, M. Milosavljevic, L. Huang, R. J. Finlay, T-H Her, J. P. Callan, and E. Mazur, "Three-dimensional optical storage inside transparent materials," Opt. Lett. **21** 2023–2025 (1996)
7. V. R. Bhardwaj, E. Simova , P. P. Rajeev, C. Hnatovsky , R. S. Taylor , D. M. Rayner, and P. B. Corkum, "Optically produced arrays of planar nanostructures inside fused silica," Phys. Rev. Lett. **96**, 057404 (2006)
8. Y. Han , X. Zhao, and S. Qu, "Polarization dependent ripples induced by femtosecond laser on dense flint (ZF6) glass," Opt. Express **19** 19150 (2011)
9. S. I. Anisimov, B. L. Kapeliovich, and T. L. Perel'man, "Electron emission from metal surfaces exposed to ultrashort laser pulses," Sov. Phys. JETP **39**, 375–377 (1974)
10. S. S. Wellershoff, J. Hohlfeld, J. Gudde, and E. Matthias, "The role of electron-phonon coupling in femtosecond laser damage of metals," Appl. Phys. A **69**, 99–107 (1999)
11. S. I. Anisimov, B. S. Luk'yanchuk, and A. Luches, "An analytical model for three-dimensional laser plume expansion into vacuum in hydrodynamic regime," Appl. Surf. Sci. **96-98** 24–32(1996)

#187454 - $15.00 USD Received 20 Mar 2013; revised 26 Apr 2013; accepted 6 May 2013; published 14 May 2013

12. M. Aden, E. Beyer, G. Herziger, and H. Kunze, "Laser-induced vaporization of a metal surface," J. Phys. D **25**, 57 (1992)
13. T. E. Itina, J. Hermann, Ph. Delaporte, and M. Sentis, "Laser generated plasma plume expansion: Combined continous-microscopic modelling," Phys. Rev. E **66**, 066406–066412 (2002)
14. P. Lorazo, L. J. Lewis and M. Meunier, "Short-Pulse Laser Ablation of Solids: From Phase Explosion to Fragmentation," Phys. Rev. Lett. **91** 225502 (2003)
15. S. I. Anisimov and B. S. Luk'yanchuk, "Selected problems of laser ablation theory," Physics - Uspekhi, **45**, 293–324 (2002)
16. F. Korte, J. Koch, and B. N. Chichkov, "Formation of microbumps and nanojets on gold targets by femtosecond laser pulses," Appl.Phys. A **79**, 879 (2004)
17. H. Tamura, T. Kohama, K. Kondo, and M. Yoshida, "Femtosecond laser induced spallation in Aliminum," J. Appl. Phys. **89**, 3520 (2001)
18. D. Bauerle, U. M. Himmelbauer, and E. Arenholz, "Pulsed laser ablation of polyimide: fundamental aspects," J. Photochem. Photobiol. A. **106**, 27–30 (1997)
19. S. Baudach, J. Bonse, J. Kruger, and W. Kautek, "Ultrashort pulse laser ablation of polycarbonate and polymethymethacrylate," Appl. Surf. Sci. **154-155**, 555-560 (2000)
20. J. Kruger, S. Martin, H. M'debach, L. Urech, T. Lippert, A. Wokaun, and W. Kautek, "Femto- and nanosecond laser treatment of doped polymethylmethacrylate," Appl. Surf. Sci. **247**, 406–411 (2005)
21. J-M Savolainen, M. S. Christensen, and P. Balling, "Material swelling as the first step in the ablation of metals by ultrashort laser pulses," Phys. Rev. B **84**, 193410 (2011)
22. B. Chimier, O. Uteza, N. Sanner, M. Sentis, T. Itina, P. Lassonde, F. Legare, F. Vidal, and J. C. Kieffer, "Damage and ablation thresholds of fused-silica in femtosecond regime, Phys. Rev. B **84**, 094104 (2011).
23. L. V. Zhigilei, E. Leveugle, B.J . Garisson, Y. G. Yingling, and M. I. Zeifman, "Computer Simulations of Laser Ablation of Molecular Substrates," Chem. Rev. **103**, 321–348 (2003)
24. B. J. Demaske, V. V. Zhakhovsky, N. A. Inogamov, and I. I. Oleynik, "Ablation and spallation of gold films irradiated by ultrashort laser pulses," Phys. Rev. B. **82**, 064113 (2010)
25. L. V. Zhigilei, Z. Lin, and D. S. Ivanov, "Atomistic modelling of short pulse laser ablation of metals: connections between melting, spallation and phase explision," J. Phys. Chem. C **113**, 11892–11906 (2009)
26. R. Herrmann, J. Gerlach, and E. Campbell, "Ultrashort pulse laser ablation of silicon: an MD simulation study," Appl. Phys. A **66**, 35–42 (1998)
27. P. Lorazoa, L. J. Lewisb, and M. Meuniera, "Picosecond pulsed laser ablation of silicon: a molecular-dynamics study," Appl. Surf. Sci. **168**, 276–279 (2000)
28. C. Cheng, A. Q. Wu, and X. Xu, "Molecular dynamics simulation of ultrashort laser ablation of fused silica," J. Phys: Conference Series **59**, 100–104 (2007)
29. C. Chen, P. Depa, J. K. Maranas, and V. G. Sakai, "Comparison of explicit atom, united atom, and coarse-grained simulations of poly(methyl methacrylate)," J. Chem. Phys. **128**, 124906 (2008)
30. B. Rethfeld, A. Kaiser, M. Vicanek, and G. Simon, "Ultrafast dynamics of nonequilibrium electrons in metals under femtosecond laser irradiation," Phys. Rev. B **65**, 214303 (2002)
31. M. Li, S. Menon, J. P. Nibarger, and G.N. Gibson, "Ultrafast Electron Dynamics in Femtosecond Optical Breakdown of Dielectrics," Phys. Rev. Lett. **82**, 2394 (1999)
32. D. S. Ivanov and L. V. Zhigilei, "Combined atomistic-continuum modeling of short-pulse laser melting and disintegration of metal films," Phys. Rev. B **68**, 064114 (2003)
33. J. Hirschfelder, C. F. Curtiss, and R. Bird, *Molecular Theory of Gases and Liquids* (Wiley, 1954 New York).
34. S. Plimpton, "Fast Parallel Algorithms for Short-Range Molecular Dynamics," J. Comp. Phys. **117**, 1 (1995)
35. E. Weinan and Li. Dong, "On the Crystallization of 2D Hexagonal Lattices," Commun. Math. Phys. **286**, 1099 (2009)
36. J-M. Guay, A. Villafranca, F. Baset K. Popov, L. Ramunno, and V. R. Bhardwaj, "Polarization dependent femtosecond laser ablation of PMMA," New. J. Phys. **14**, 085010 (2012)
37. M. E. Povarnitsyn, T. E. Itina, M. Sentis, K. V. Khishchenko, and P. R. Levashov, "Material decomposition mechnaisms in femtosecond laser irradiation with metals," Phys. Rev. B **75** 235414 (2007)
38. E. Leveugle, D. S. Ivanov, and L. V. Zhigilei, "Photomechanical spallation of molecular and metal targets: molecular dynamics study," Appl. Phys.A **79** 1643–1655 (2004)
39. D. S. Ivanov, Z. Lin, B. Rethfeld, G. M. O'Connor, T. J. Glynn, and L. V. Zhigilei, "Nanocrystalline structure of nanobump generated by localized photoexcitation of metal film," J. Appl. Phys. **107**, 013519 (2010)
40. M. B. Agarnat, S. I. Anisimov, S. I. Ashikov, V.V. Zhakhovskii, N. A. Inogamov, K. Nishihara, Yu. V. Petrov, V. E. Fortov, and V. A. Khokhlov, "Dynamics of plume and crater formation after action of femtosecond laser pulse," Appl. Surf. Sci. **253** 6276-6282 (2007)

#187454 - $15.00 USD Received 20 Mar 2013; revised 26 Apr 2013; accepted 6 May 2013; published 14 May 2013

1. Introduction

Laser ablation is often associated with removal of material and is widely used for surface patterning and thin film fabrication. The former is used to dramatically alter wetting [1], mechanical, electrical and optical properties of materials [2]. Laser ablation has been studied in diverse materials using a range of wavelengths (ultraviolet to infrared), pulse durations (nanoseconds to femtoseconds) and repetition rates (kHz to MHz) for micro-fabrication to produce surface features with suitable texture and less contamination compared to other methods. More recently, femtosecond lasers have evolved as an advanced machining tool for material processing with nanometer precision [3, 4] enabled by localized energy deposition due to highly nonlinear multiphoton interaction of light with matter. As a result, they provide high intensities needed to ablate material from surface quickly and cleanly, without damaging the surrounding regions. To-date, they have been employed to induce refractive index modification in 3D [5], voids [6], phase transitions and periodic nanostructures on the surface and in the bulk [7, 8].

Several studies, both experimental and theoretical, have focused on the underlying physics of femtosecond laser-matter interaction to optimize and develop various applications of laser ablation. Measurement of ablation depth/etch rates, surface swelling, melting and thermal damage combined with investigation of ablation dynamics using pump-probe techniques provided some mechanistic insights into the process. The highly non-equilibrium character of the laser-induced processes are often described by a two-temperature model that couples electron temperature with the lattice temperature [9, 10]. Subsequent expansion of evaporated material plume and the formation of plasma within the plume are studied using hydrodynamic models [11, 12] and Monte Carlo simulations [13, 14].

In spite of these advances, the mechanisms responsible for material removal by ultrashort laser pulses still remain controversial [15]. In addition, the question of whether ablation starts with direct material removal or with surface swelling followed by material ejection has never been clearly addressed in bulk materials. Surface swelling has mostly been observed in thin metal [16, 17] and polymer films and has been attributed to spallation - strong mechanical effects that play a role during laser excitation resulting in physical separation of a thin layer from the substrate. Polyimide foils under nanosecond UV-laser induced surface irradiation [18] have shown three different regimes with increasing fluence such as, (a) real material removal (ablation), (b) swelling of the irradiated area above the level of the untreated surface (hump formation) and (c) lowering of the irradiated area below the level of the untreated surface (dent formation). Polycarbonate and PMMA (both doped and undoped) foils have also been investigated under femtosecond laser irradiation and surface swelling always accompanied ablation [19, 20]. Recently, surface swelling has been reported as the first step in ablation of bulk metals [21] and has also been observed in ablation of fused silica glass [22].

Microscopic models based on molecular dynamics (MD) approach [23] were employed to investigate fast dynamic material response to short pulse laser irradiation in metal films [24, 25], semiconductors [26, 27] and dielectrics [28]. The MD approach is also an important method in polymer studies [29]. In MD simulation, the atoms interact with each other via a predefined potential, and their motion is tracked at every time step. MD simulations in metals suggested spallation is initiated by void nucleation and growth, both in size and numbers, followed by void coarsening and coalescence [25]. Long after the interaction of the incident laser pulse, a thick layer of material re-solidifies in a foamy state with holes and voids, leaving a bump, which extends above the original surface level [21]. However, a complete and coherent picture of how ablation is established in bulk materials especially in polymers is yet to emerge.

In this paper, we report ablation of bulk PMMA with a single femtosecond laser pulse and show that swelling of the material surface always precedes any large scale material ejection. We show that ablation evolves from surface swelling as higher pulse energies puncture a hole at the

#187454 - $15.00 USD Received 20 Mar 2013; revised 26 Apr 2013; accepted 6 May 2013; published 14 May 2013

centre of the swollen structure that gradually increases in size. Concurrently, the height of the swollen structure decreases while the depth of the ablated hole increases. We demonstrate that the pulse energy at which the ablated hole size coincides with size of swelling is $\sim$ 1.5 times that of the threshold for surface swelling and is independent of laser polarization suggesting existence of two energy thresholds corresponding to surface swelling and material removal being dominant. MD simulation of interaction of femtosecond pulses with PMMA in 2D using a computational cell consisting of 40 million particles with dimensions of $\sim 2\mu$m$\times 2\mu$m demonstrate void formation and material swelling are important mechanisms of temperature equilibration at the surface of the laser-heated sample.

2. Experiment

800nm light from a Ti:Sapphire laser system operating at a repetition rate of 5 kHz and producing 45 fs pulses with a peak energy of 0.5 mJ, was focused on the surface of optically polished PMMA samples (12.5$\times$12.5$\times$1.7 mm) by a 0.25NA (10$\times$) microscope objective. The back aperture of the microscope objective (8 mm) was slightly overfilled to minimize alignment errors. The position of the laser focus relative to the sample surface was accurately determined by imaging the back reflected light with a CCD camera at very low pulse energies below the ablation threshold. After locating the surface of PMMA, the glass plate at 45°, used for directing the back reflected light, was removed in order to avoid distortion of the incident polarization. A thin broadband beam sampler at the output of the laser directed a small fraction of the beam into a single-shot autocorrelator to monitor the pulse duration continuously. The pulse duration at the back aperture of the objective was measured to be 70fs after propagating through all the optics. The pulses were not pre-chirped.

Single femtosecond pulses were selected by operating the laser in an external trigger mode. A gradient neutral density filter was used to vary the pulse energy from 200nJ to 5μJ. The pulse energy was varied in steps of 50nJ up to 1μJ and in steps of 100nJ thereafter. A calibrated fast photodiode operating in the linear regime monitored the incident power. The incident pulse energies were measured after the microscope objective taking into account the transmission and reflection losses of all the optics. The polarization of the incident light was varied by a half-waveplate (quarter- waveplate) to obtain linearly (circularly) polarized light.The PMMA sample was mounted on three-axis translation stages with a resolution of 50nm along the lateral dimensions (X, Y) and 100 nm along the axial direction (Z).

The laser-ablated regions were characterized by a scanning electron microscope (SEM) after gold coating the PMMA surface with a thin layer (few nanometers) to make them conductive. All SEM images were taken with the electron beam perpendicular to the sample (zero tilt). The spot size was obtained from the slope of semi-logarithmic plot of the squared diameter of the modified region measured with the SEM as a function of pulse energy. We obtained a Gaussian beam radius of 2.7$\pm$0.2μm for the 0.25NA microscope objective (close to the diffraction-limited beam radius of $\sim 2\mu$m) and used it to calculate the laser fluence values. The lowest energy at which ablation features were visible under SEM was defined as the threshold value.The single shot ablation threshold of PMMA was determined to be 0.6μJ corresponding to a laser fluence of 2.6 J/cm^2, in good agreement with the published data [19].

Laser induced surface topology was investigated by an Atomic Force Microscope operating in contact mode with a pyramidal cantilever having a half-cone angle of 35°, tip height of 3.5μm and a spring constant of 69$\pm$1pN/nm tracing the sample with $<$10nN in radius of curvature. Images were captured with a relative tip speed of 1μm/sec. The typical lateral and vertical resolutions were 30nm and 0.1nm respectively.

#187454 - $15.00 USD Received 20 Mar 2013; revised 26 Apr 2013; accepted 6 May 2013; published 14 May 2013

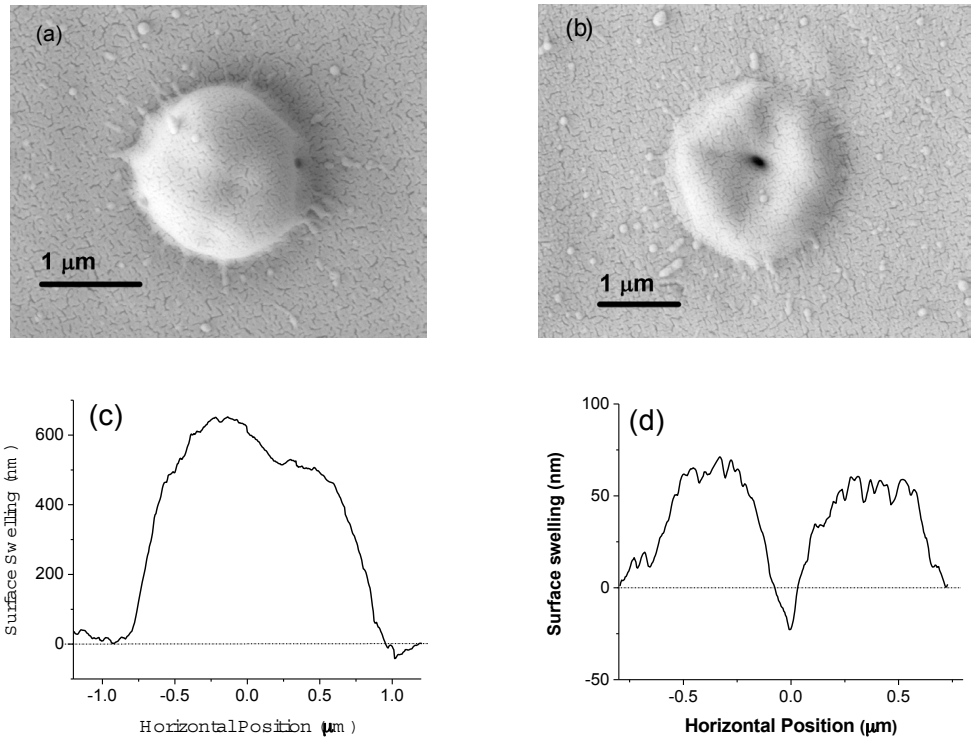

Fig. 1. Surface topography induced by a single femtosecond laser pulse in bulk PMMA. SEM images of material swelling produced by (a) circularly polarized light with a pulse energy of 640 nJ and (b) linearly polarized light with a pulse energy of 650 nJ. Respective AFM cross-sections are shown in (c) and (d) with the dashed line representing the surface before laser-irradiation.

2.1. Results

Figure 1(a) shows SEM image of PMMA surface irradiated by a single, circularly polarized femtosecond pulse of energy 640nJ. This pulse energy is slightly above the damage threshold in PMMA below which no observable surface effects could be discerned in SEM. A smooth, near circular dome like structure is formed that extends to $\sim$1.8μm with a tiny nanopore at the bottom of the dome to the right. The dome height is $\sim$600nm as shown in Fig. 1(c), measured by an AFM. When pulse energy is slightly increased the dome like structure collapses after a hole is formed at the centre as shown in Fig. 1(b). Although the laser polarization is linear in this case similar results are obtained with circular polarization as shown below. AFM measurements (shown in Fig. 1(d)) indicate a height of 75nm with a hole size of $\sim$110nm.

These results suggest that surface swelling is the first step in the ablation of materials with femtosecond lasers and that ablation proceeds with perforation of the dome like swollen surface structure. Figure 1(b) also suggests the region underneath the swollen structure is hollow resulting in the collapse of the dome when punctured at higher pulse energy. Presence of radial ejection patterns at the edges of the dome like structure in both images along with nanodroplets in the adjacent regions indicate that surface swelling arises from molten state of the material that is re-solidified possibly due to rapid cooling during expansion.

Figure 2 shows the evolution of the laser damaged surface of PMMA from surface swelling to ablation crater with increasing pulse energy for a single laser pulse of circular polarization.

#187454 - $15.00 USD Received 20 Mar 2013; revised 26 Apr 2013; accepted 6 May 2013; published 14 May 2013

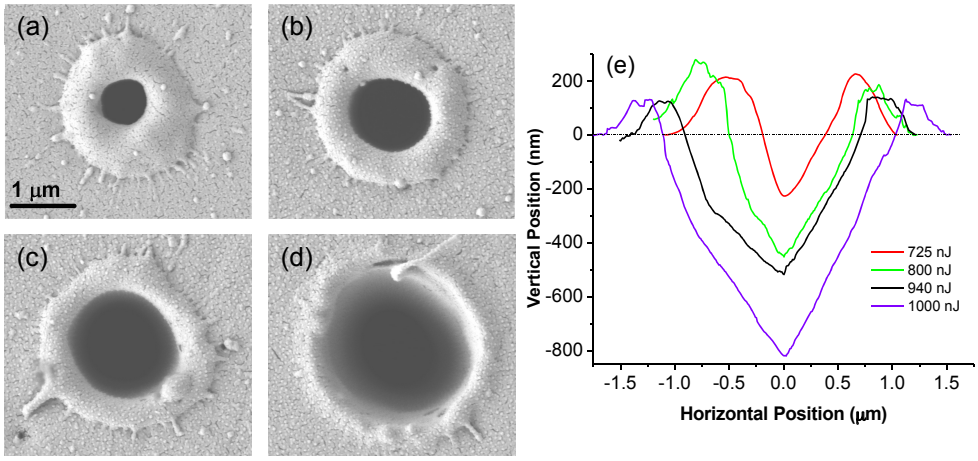

Fig. 2. SEM images showing evolution of the ablated hole within the swollen surface in PMMA induced by a single, circularly polarized femtosecond laser pulse with pulse energies of (a) 725 nJ, (b) 800 nJ, (c) 940 nJ and (d) 1 μJ corresponding to laser fluences of 3.2, 3.5, 4.1 and 4.4 J/cm^2 respectively. (e) Corresponding AFM cross-sections showing dependence of swelling and ablation hole dimensions for same incident pulse energies.

At pulse energies higher than 640 nJ, a pore formed at the centre of the dome like swollen structure renders it a doughnut shape (Fig. 2(a)). As pulse energy increases, the extent of the laser modified region and the overall pore size increases but the width of the doughnut rim decreases (Fig. 2(b) and 2(c)). When pulse energy is one half of the damage threshold the rim like structure surrounding the ablated hole vanishes as the hole size coincides with the size of swelling. Figure 2(e) shows the corresponding AFM cross-sections. Material removal commences at a pulse energy of $\sim$650 nJ (Fig. 1(b)) and at 725 nJ, the depth of the ablated hole is $\sim$225 nm with an annular protrusion of $\sim$225nm and a width of $\sim$ 640 nm. With rising pulse energy, the ablated hole diameter and depth increases while the height of the annular protrusion decreases.

The dependence of ablated hole and swelling width on incident pulse energies is shown in Fig. 3(a) for linear and circular polarizations. For both polarizations, the ablated hole and swelling size increases almost linearly with applied pulse energy up to 1.1 μJ. However, the hole size increases at a much faster rate of $\sim$6.5nm/nJ compared to $\sim$3nm/nJ rate at which the swelling increases. Beyond 1.1μJ, both ablated hole and swelling size grow at a slower rate of $\sim$0.8nm/nJ. Figure 3(b) shows the comparison between AFM cross-sections for circularly and linearly polarized light at similar pulse energies (725 nJ and 690 nJ respectively) suggesting no polarization dependence of surface swelling and subsequent material ejection at higher pulse energies.

3. Numerical simulations

The femtosecond laser ablation process can be characterized by at least three distinct stages separated by their time-scales. (1) Laser-matter interaction stage where plasma is formed and heated due to the collisional absorption processes on a time-scale on the order of several tens of femtosecond, determined primarily by the laser pulse duration. (2) Collisional transfer of energy from the laser-produced electron gas to the molecular structure with a characteristic time on the order of several hundred femtoseconds [30]. This is somewhat longer than the characteristic electron recombination time scale ($\sim$one hundred femtoseconds [31]), which thus

#187454 - $15.00 USD Received 20 Mar 2013; revised 26 Apr 2013; accepted 6 May 2013; published 14 May 2013

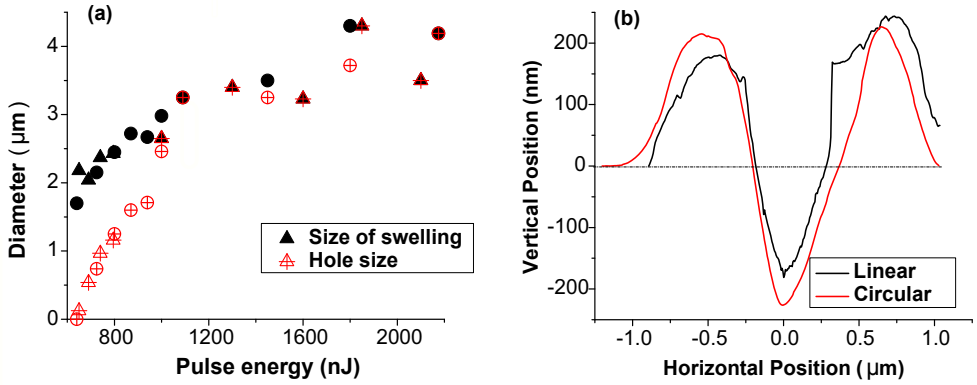

Fig. 3. (a) Dependence of diameter of the ablated hole (open symbols) and swelling (closed symbols) on incident pulse energies for linear (up-triangles) and circular (circles) polarizations. (b) Comparison of AFM cross-sections for circularly and linearly polarized light at pulse energies of 725 nJ and 690 nJ, respectively.

appears to be the dominant mechanism of energy transfer from the laser-produced plasma to the molecular structure. (3) Temperature equilibration process with a characteristic time-scale of picosecond to nanoseconds determined by the speed of sound in PMMA ($\sim 2.7 \times 10^3$ m/s $=$ $2.7\,\mu$m/ns) that can lead to surface swelling, material ablation and formation of mechanical defects.

Below we present phenomenological simulations aimed at understanding the general mechanics of thermal processes leading to formation of the dome-like structures and ablation craters in bulk samples. We consider only the third stage of the interaction, assuming that the first two stages have produced a certain temperature profile in the sample that is taken as initial condition in the simulations. We also assume that the particle density profile is minimally perturbed during the first two fast processes. As a result, the initial particle density distribution is considered to be uniform within the sample.

3.1. Methods

We use molecular dynamics (MD) approach to model interaction of femtosecond laser pulses with PMMA as it is naturally capable of describing the non-equilibrium phase transition processes at atomic level. In contrast, hydrodynamic models that are typically used to describe thermal processes in bulk samples have been shown to encounter serious challenges when extended to ultrafast laser ablation [32] due to fundamental difficulties in describing highly non-equilibrium phase transition processes along with the necessity to resolve microscopic processes.

Several MD models, differing in accuracy and computational requirements, have been developed for microscopic description of polymers and their properties under a wide range of conditions [29]. In principle, MD models can also support polymer chain-break processes with a little overhead. However, a more-or-less realistic description of polymer chains necessarily requires an actual 3D representation. MD simulations in bulk in 3D is a computationally daunting task even for largest supercomputers employing the coarse-gain MD model. To reduce computational requirements, cell dimensions on the order of few 10's to 100's of nm (much smaller than the laser spot size) are typically used in 3D with approximately few hundred thousand particles. As a result plane wave approximation is used for the incident light ignoring the gaussian spatial profile of the laser.

#187454 - $15.00 USD Received 20 Mar 2013; revised 26 Apr 2013; accepted 6 May 2013; published 14 May 2013

In this paper, we use a 2D phenomenological model with computational cell dimensions on the order of the laser spot size that enables us to consider the spatial profile of the laser. The interaction between individual atomic entities is described by the Lennard-Jones potential

$$V(r) = 4\varepsilon_0\Big[\Big(\frac{\sigma}{r}\Big)^6 - \Big(\frac{\sigma}{r}\Big)^{12}\Big], \tag{1}$$

where σ is the characteristic length and ε_0 the characteristic depth of the potential. In this way, we only expect to learn about the qualitative dynamics of ablation process, while the particular details such as elastic properties of polymers due to their chain structure at microscopic level and formation of volatile compounds due to chain breaking will be inevitably lost. Coarse grain techniques are often used where few atoms, monomers or even the whole molecular chain are grouped together to reduce computational requirements. The impact of reduced chemical detail on structural and dynamical properties of PMMA has recently been investigated where different approximations used in the MD simulations have been shown to provide adequate agreement with experimental data [29]. With the use of atomic picture in our simulations we anticipate the loss of details not to be detrimental in extracting qualitatively the thermo-mechanical properties of polymers.

Since simulations are phenomenological, the particular values of ε_0 and σ can vary. For different molecules, ε_0/k_B can be on the order of $10^2 - 10^3$ K, where k_B is Boltzmann constant, and σ can be on the order of $0.25 - 0.6$ nm [33]. The actual simulations were performed using dimensionless units. The dimensionless coordinate, time and temperature are, corrsepondingly, $\tilde{r} = r/r_0$, $\tilde{t} = t/t_0$ and $\tilde{T} = T/T_0$, where $r_0 = \sigma$, $t_0 = \sqrt{m\sigma^2/\varepsilon_0}$ and $T_0 = \varepsilon_0/k_B$. For example, if one uses $\sigma = 0.3$ nm, $\varepsilon_0/k_B = 10^3$ K and $m = 18\,m_p$, where m_p is the proton mass, that is close to parameters of water, one obtains $x_0 = 0.3$ nm, $t_0 = 0.4$ ps and $T_0 = 1000$ K.

In our simulations, we use the freely available LAMMPS code (http://lammps.sandia.gov [34]). We use $\sim 4\times 10^7$ particles on a 2D hexagonal lattice occupying $\sim 6000\times 6000\,\sigma^2$ area ($\sim 2\times 2\,\mu$m for $\sigma = 0.3$ nm). A single simulation run consists of two stages. Initially, the atomic entities are motionless and located at the nodes of the lattice in the equilibrium state. During the first stage of simulations, the sample is annealed in the Nose-Hoover thermostat with a slowly increasing temperature, until the room temperature T_r is reached ($T_r \sim 0.75\,T_m$, where T_m is the melting temperature, equal to $\sim 0.41T_0$ for the hexagonal 2D lattice [35]). Thus, an initial unperturbed equilibrium state is created.

At the beginning of the second stage of simulation, particle velocities are scaled up by a factor proportional to the square root of temperature profile $T(\vec{r},0)$ corresponding to the non-equilibrium configuration created by the laser pulse (Fig. 4 at $t = 0$). The particles are then propagated self-consistently by the LAMMPS NVE solver, while a thin layer near $y = y_{min}$ and $y = y_{max}$ is kept at constant temperature to mimic a bulk thermal reservoir. In a typical simulation, the second stage takes $\sim 10^7$ time steps to reach a stable equilibrium (completely frozen state) for a single time step $\delta t = t_0/400$.

The temperature profile $T(\vec{r},0)$ is determined by the spatial distribution of the energy transferred from the laser beam to the molecular structure:

$$T(\vec{r},0) \approx T_r + \delta\mathscr{E}_i + \delta\mathscr{E}_{ca}, \tag{2}$$

where $\delta\mathscr{E}_i$ is the laser pulse energy transferred to the electrons in the ionization process and $\delta\mathscr{E}_{ca}$ is the pulse energy absorbed by electrons in the collisional absorption process. T_r is the room temperature.

Assuming that multi-photon ionization is the dominant ionization process in the near-threshold interaction and perturbation of the laser propagation by the resultant plasma is negli-

#187454 - $15.00 USD Received 20 Mar 2013; revised 26 Apr 2013; accepted 6 May 2013; published 14 May 2013

gible, one can write

$$\delta\mathscr{E}_i \propto \left(\frac{I(\vec{r})}{I(\vec{r}_f)}\right)^N, \tag{3}$$

where $I(\vec{r})$ is the spatial profile of the unperturbed laser pulse, $\vec{r}_f$ is the position of the laser best focus and N the order of multi-photon absorption process, $N = 3$ in the case of PMMA. In Eq. (3), a simple rate equation for multi-photon ionization rate is used. In order to estimate the extent of the laser profile perturbation by the plasma that is formed during the interaction one can calculate the energy density required to generate plasma of critical electron density ($n_{cr} = 1.75 \times 10^{21}\,\mathrm{cm}^{-3}$ for the laser wavelength $\lambda = 0.8\,\mu$m in vacuum):

$$W_{ion} n_{cr} \approx 4\,\mathrm{eV} \times 1.75 \times 10^{21}\,\mathrm{cm}^{-3} = 7 \times 10^{21}\,\mathrm{eV/cm}^3, \tag{4}$$

where W_{ion} is the ionization potential. The heat capacity of PMMA at room temperature is $\sim 1\,\mathrm{J/(cm^3K)} \approx 6 \times 10^{18}\mathrm{eV/(cm^3K)}$. Thus, the energy required to produce plasma of critical density can be sufficient to locally heat the sample by more than 1000 K. Our simulations below indicate that significant thermal processes can take place in the sample heated by (1 – 1.5) T_r above the unperturbed temperature, i.e., by ∼300–400 K. Since a part of this energy is produced in the collisional plasma heating process, we conclude that the plasma density in the near-threshold regime is well below critical density that justifies our assumption of negligible perturbation of the laser propagation by the generated plasma.

The collisional absorption of laser energy by plasma is a nonlinear process that is dependent on the distribution function of electrons at each time moment. Thus, $\mathscr{E}_{ca}$ is dependent not only on the produced plasma density n, but also directly on the laser intensity. However, since the inverse Bremmstrahlung absorption is only one of the energy transfer mechanisms from the laser pulse and nonlinearity in $n(I)$ is very strong, the extra dependence on the laser intensity due to the details of the collisional absorption process is expected to result only in perturbation of the overall laser energy deposition profile in the sample. In this way, to keep our parameter space small, we assume, similar to Eq. (3),

$$\delta\mathscr{E}_{ca} \propto \left(\frac{I(\vec{r})}{I(\vec{r}_f)}\right)^N. \tag{5}$$

The overall temperature profile in the sample assumed at the beginning of the thermal stage is thus

$$T(\vec{r},0) \approx T_r \cdot \left[1 + \alpha \cdot \left(\frac{I(\vec{r})}{I(\vec{r}_f)}\right)^N\right], \tag{6}$$

where α is a parameter of simulations. The particle velocities used at the second stage of simulation are therefore scaled up by factor $\sqrt{1 + \alpha \cdot \left(I(\vec{r})/I(\vec{r}_f)\right)^N}$.

3.2. Simulations results

Dynamics of a typical bump formation process is illustrated in Fig. 4 for $\alpha = 1.45$. The laser is incident on the sample surface at x/σ = 0. The temperature distribution follows the energy deposition and spatial profile of the laser and is highest at y/σ = 0 and penetrates deeper into the sample. In a few tens of t_0, corresponding to few picoseconds after the start of simulation (represented by t_w obtained for a particular choice of parameters) , the initial non-equilibrium process gives rise to a strong pressure shock that propagates with a supersonic velocity outwards from the hot area and eventually decays, after several subsequent reflections from the boundaries of the simulation sample. The shockwave traverses the simulation domain in about 150 ps.

#187454 - $15.00 USD Received 20 Mar 2013; revised 26 Apr 2013; accepted 6 May 2013; published 14 May 2013

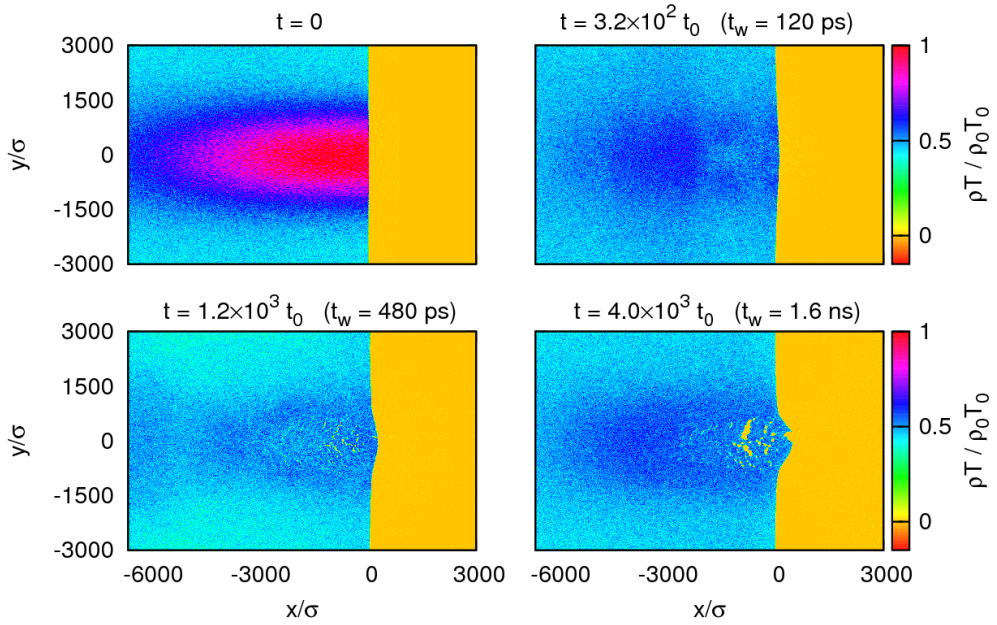

Fig. 4. (Characteristic dynamics of thermal processes and bump formation in the laser-heated sample. Density weighted temperature profiles are shown at different time steps for $\alpha = 1.45$. The laser is incident from the right on the sample surface located at x/σ = 0 and centred at y/σ = 0. Simulation domain size of x/σ = y/σ = 6000 corresponds to sample dimension of $\sim 2\mu$m$\times 2\mu$m. Time t_w is obtained from dimensionless unit for a particular choice of parameters specified in the text.

The next state of equilibration, that can correspond to few tens of picoseconds, is characterized by formation of gaseous nanopores inside the overheated area and its rapid cooling (Fig. 4, $t = 3.2 \times 10^2 t_0$). The temperature profile in Fig. 4 at $t = 3.2 \times 10^2 t_0$ shows formation of nanopores in a region that is initially the hottest with corresponding temperatures that are cooler than the surrounding material. Thus, the nanopores formation is an important mechanism of temperature equilibration. Near the boundary of the sample, pressure gradient leads to expansion of the porous material outwards that leads to formation of a bump at the sample surface (Fig. 4, $t = 1.2 \times 10^3 t_0$). This process is accompanied by the growth of the nanopores, that eventually coalesce to form larger pores (Fig. 4, $t = 4.0 \times 10^3 t_0$). The surface bump at this stage develops large mechanical defects that, depending on the deposited energy, either increases further at later time and result in an open crater or freeze and form the swollen structure with a perforated hole that is seen in the experimental images described in the previous section. The height of the bump/swelling increases at a rate of $\sim$13 nm for every 100 ps up to few ns in time. Beyond 10 ns simulations do not show any changes in the surface topography although thermal processes continue for longer times.

Figure 5 shows the density profiles of the interaction region after $2.5 \times 10^4 t_0$ (corresponding to ten to few tens of ns after the interaction that is long enough for re-solidification to occur) for different values of the simulation parameter α. For $\alpha = 1.1$, only nanopores and irregularities appear to be present under the sample surface that appear as brighter regions in the figure. A small crack visible near the surface can be attributed to the dimensionality of the computation cell (relatively small size of our sample that is comparable to the laser spot size) and the stiffness of the sample surface. The shock produced by the initial temperature gradient could not be

#187454 - $15.00 USD Received 20 Mar 2013; revised 26 Apr 2013; accepted 6 May 2013; published 14 May 2013

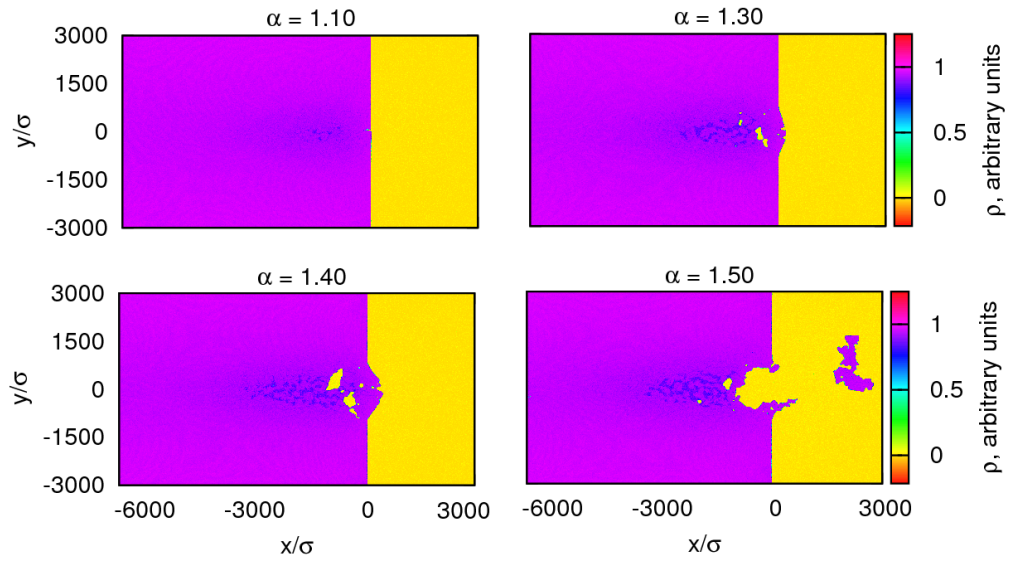

Fig. 5. Particle density profiles $2.5 \times 10^4 t_0$ (~ 10 ns) after the interaction of light with the sample for different values of α corresponding to different pulse energies.The laser is incident from the right on the sample surface located at x/σ = 0 and centred at y/σ = 0. Dimensions of sample used in the simulation are $\sim 2\mu$m$\times 2\mu$m corresponding to x/σ = y/σ = 6000.

completely overcome by the Lennard-Jones walls of the simulation domain. At higher α when the material becomes softer the crack does not appear.

For $\alpha = 1.3$ some of the irregularities in the density coalesce to form sub-surface voids that leads to the formation of a small bump at the sample surface. Mechanical stretching of the thermally softened sample surface leads to formation of micropores on the swollen surface. As α is increased to $\alpha = 1.4$, the sub-surface voids and the surface bump grow in size. A deeper and larger hole is formed on the surface bump that can be interpreted as a central pore observed in the experiment. As the α is increased to $\alpha = 1.5$, the internal pressure in the sample becomes sufficiently large to detach large chunks of material from the sample creating an ablation crater with a porous structure at its bottom that has previously been observed in experiments on PMMA [36].

4. Discussion

Surface swelling induced by ultrashort laser pulses that we observed in bulk PMMA is not the same as that has previously been observed in metal films [16, 17]. There the mechanism is attributed to spallation – a photomechanical process where a reflected pressure wave leads to material ejection typically at the back surface of the sample. MD simulations of small material slabs provided insights into the thermo-mechanical dynamics of irradiated films including coupling-decoupling of ablation and spallation processes [24]. However, the bulk nature of our sample excludes the influence of a substantial reflected pressure wave.

Our simulations demonstrate formation of nanopores in the subsurface region of highly excited material due to the interaction of intense short pulses with the sample. Pressure gradients near the sample boundary causes the porous material to expand outwards forming a bump at the sample surface. This is accompanied by growth and coalescence of voids in the subsurface region. The evolution of voids determined by the competition between the laser-induced stresses

#187454 - $15.00 USD Received 20 Mar 2013; revised 26 Apr 2013; accepted 6 May 2013; published 14 May 2013

and thermal softening of the irradiated surface can lead to spallation, fragmentation and ejection of material. This is similar to front-surface laser spallation predicted by hydrodynamic [37] and MD modelling [25, 38, 39].

Simulations also suggest surface swelling to increase with α (pulse energies) up to a certain value beyond which mechanical stretching of the sample surface leads to formation of a central pore (Fig. 5(c)) as observed in experiments. Further increase in α (not shown) leads to an increase in the hole size. At high α, material removal becomes dominant and surface swelling can no longer be observed. The α at which hole and swelling sizes coincide is 1.3 times the threshold α at which only swelling is observed. Experimentally, this ratio was found to be 1.5. Time-resolved measurements of femtosecond laser induced surface swelling in metal foils have observed a similar threshold fluence that separates the regime where a dome like structure (unbroken shell) is formed from the regime with the dome (shell) having an aperture [40].

Our simulations in bulk material, albeit in 2D, indicate that a two phase expanding liquid-vapour mixture fills the volume between the shell and bottom of the crater consistent with other simulations [25, 40] and experiments [21] carried out in metal foils. However, the collapse of dome like structure in Fig. 1(b) at slightly higher fluence suggests the inside is hollow. This could be specific to PMMA and other polymers. In addition to the laser-induced subsurface liquid-vapour mixture that expands, another potential source of gaseous products can be polymer fractionation by CO-O bond breaking [19]. Irrespective of the relative contributions, localized bursting of the expanding surface results in collapse of the dome structure.

5. Conclusion

We demonstrate that surface swelling is the first step in interaction of intense femtosecond pulses with bulk dielectrics. This is followed by material ejection and ablation only when laser fluence/pulse energy is increased. The threshold fluence at which ablation becomes dominant with no reminiscents of surface swelling is approximately one and half times the threshold for surface swelling and is independent of laser polarization. These results have implications in ultrafast micro-machining applications when combined with previous observations of polarization dependent elongation of ablated holes at fluences greater than twice the ablation threshold [36]. There appears to be a small range of laser fluences where clean holes and cuts are feasible. At low fluences, surface swelling dominates and at high fluences ablation dominates but polarization effects can become prominent. Detailed time-resolved experiments extending to longer times will shed more light on swelling dynamics. Our molecular dynamics simulations provide physical insight into swelling dynamics showing that (a) bump formation is not connected to laser induced shock but to the formation of porous structure below the sample surface, and (b) no significant evaporation occurs from the surface at threshold fluences. Large scale simulations that take into account the molecular structure of PMMA and involves sample sizes comparable to the laser spot size are essential to gain further insight into the nonlinear interaction of light with matter.

Acknowledgments

The authors acknowledge the financial support from Natural Science and Engineering Research Council of Canada, Canada Research Chairs, Canadian Foundation for Innovation and Ontario Ministry of Economic Development and Innovation. Z.A is supported by NSERC-CREATE in Quantitative Biomedicine fellowship. Computations were performed on the Southern Ontario Smart Computing Innovation Platform (SOSCIP) BlueGene/Q supercomputer located at the University of Toronto's SciNet HPC facility.

#187454 - $15.00 USD Received 20 Mar 2013; revised 26 Apr 2013; accepted 6 May 2013; published 14 May 2013